Eur. Phys. J. B **14**, 633–637 (2000)

THE EUROPEAN PHYSICAL JOURNAL B

EDP Sciences

Phase transitions in $Sr_{0.61}Ba_{0.39}Nb_2O_6$:$Ce^{3+}$: II. Linear birefringence studies of spontaneous and precursor polarization

P. Lehnen[1], W. Kleemann[1,a], Th. Woike[2], and R. Pankrath[3]

[1] Laboratorium für Angewandte Physik, Gerhard Mercator-Universität, 47048 Duisburg, Germany
[2] Institut für Kristallographie, Zülpicher Straße 49b, Universität zu Köln, 50674 Köln, Germany
[3] Fachbereich Physik, Universität Osnabrück, 49069 Osnabrück, Germany

Received 1 October 1999

Abstract. The linear birefringence (LB) of $Sr_{0.61-x}Ba_{0.39}Nb_2O_6$:$Ce_x^{3+}$ (SBN61:Ce) has been measured as a function of temperature within the range of $78 \leq T \leq 850$ K. Large tails have been observed above the ferroelectric phase transition temperatures $T_c = 350$, 328, 320 and 291 K for the concentrations $x = 0, 0.0066$, 0.0113 and 0.0207, respectively. Within an Ornstein-Zernike analysis the critical exponents γ, ν and β are determined. It suggests that pure SBN61 belongs to the 3D Ising universality class. Doping with Ce^{3+} ions, which seem to act as random fields, enhances the relaxor properties. The critical exponents γ and ν of SBN61:Ce shift against those of the three-dimensional random-field Ising model.

PACS. 64.60.Fr Equilibrium properties near critical points, critical exponents – 77.80.Bh Phase transitions and Curie point – 77.84.Dy Niobates, titanates, tantalates, PZT ceramics, etc.

1 Introduction

In this paper the properties of the tungsten-bronze ferroelectric material strontium-barium niobate $Sr_{1-y}Ba_yNb_2O_6$ (SBN) are discussed. SBN is an interesting material due to the variety of its potential applications, particularly in the areas of pyroelectricity [1], piezoelectricity [2], electro-optics [3,4], photorefractive optics [5–8] and non-linear optics [9].

For a concentration $1 - y = 0.61$ the compound (SBN61 for short) is congruently melting [10]. Hence, large crystals of high optical quality can be grown. Above the ferroelectric phase transition temperature, $T_c = 350$ K for pure SBN61, the structure is tetragonal (4/mmm). Below T_c it remains tetragonal (4 mm) and reveals spontaneous polarization **P** along the c axis. Doping with Ce^{3+}, where only the Sr^{2+} sites are substituted [11], strongly lowers the phase transition temperature [12]. The influence of the dopants, due to charge disorder, and the open structure of SBN favor the formation of local polar regions even in the paraelectric regime. Evidence of such precursor phenomena in SBN has already been obtained, *e.g.* from Raman scattering [13] and second-harmonic-generation [14,15] studies. In previous studies we investigated the appearance of clusters and domains both in the paraelectric precursor and in the ferroelectric regime of SBN61:Ce^{3+} using dielectric spectroscopy [16] and atomic force microscopy [17]. Strong evidence of dynamic nanodomains above T_c, but static ferroelectric domains below T_c has shed some light on the peculiarity of the phase transition in this system.

The one-dimensional order parameter and the existence of random fields (RFs), due to the above mentioned charge disorder, suggest to consider SBN:Ce as an example of the three-dimensional (3D) random-field Ising model (RFIM). Although the RF mechanism has been proposed to play an important role to understand the properties of relaxors [18], its relevance is not easy to demonstrate. In prototypical systems like $PbMg_{1/3}Nb_{2/3}O_3$ (PMN) with cubic symmetry and nearly continuous order parameter symmetry both random bonds and RFs [19] are expected to destroy the phase transition. The resulting glassy or domain states, respectively, are difficult to distinguish [18]. Such systems rather possess hybrid properties and may best be described by a spherical random bond-random field model as proposed previously [20]. This situation should change, however, for a system like SBN61 with large order parameter anisotropy. Its tendency to form RF stabilized domain states should vanish in the limit of weak RFs [19]. Under the assumption of sufficiently weak bond randomness only the RFs should determine the asymptotic fixed point. Hence, modified critical behaviour should eventually be observable outside some rounding region in the vicinity of T_c [21].

[a] e-mail: wolfgang@kleemann.uni-duisburg.de

In order to study the RF critical behaviour we have systematically measured the temperature dependence of the linear birefringence (LB) of pure and Ce^{3+} doped SBN61 for concentrations $x = 0.0066$, 0.0113 and 0.0207. In contrast with ac susceptibility measurements as experienced in our previous paper [16], the LB method is quasistatic and probes near-equilibrium properties. Rounding effects [16] are largely avoided thus providing access to critical behaviour close to T_c. An Ornstein-Zernike analysis of the LB data shows the concentration dependent critical behaviour of SBN61. This gives a hint at the effectiveness of RFs in the system. It is expected that an increasing Ce^{3+} concentration increases the average amplitude of the RFs and thus causes a crossover into RFIM critical behaviour.

2 Experimental procedure

Pure SBN61 and Ce^{3+} doped crystals were grown by the Czochralski technique. Large and clear optical-quality single crystal bars have been obtained. Platelet-shaped samples with dimensions of about $5 \times 5 \times 1$ mm^3 with the polar c-axis ([001] direction) parallel to the long edges of the plates were cut and polished to optical quality. The principal LB, Δn_{ac}, was measured with a computer-controlled modulation method [22] at $\lambda = 589.3$ nm on a microscopically selected, fixed sample area of 40×40 μm^2. Temperatures between 77 and 850 K were achieved using a variable temperature stage. The LB was measured starting from 78 K while heating at a rate of less than 1 K/min. The temperatures were measured with a calibrated Pt-resistance with a resolution of 0.01 K.

3 Experimental results and data evaluation

Figure 1 shows the temperature dependence of the LB of SBN61:Ce^{3+}. The zero points at $T = 78$ K of the raw data (inset) were arbitrarily chosen. The dashed line represents the thermo-optic contribution Δn_{ac}^{th} of the LB in the absence of any ferroelectric correlations. It is described within the indicatrix formalism of crystal optics [23]. The variation of the principal dielectric impermeability components $(1/n^2)_{ij}$ is given by the elasto-optic effect

$$\delta\left(1/n^2\right)_{ij} = p_{ijkl}\alpha_{kl}\Delta T, \tag{1}$$

where α_{kl} are the thermal expansion coefficients and $\alpha_{kl}\Delta T = \varepsilon_{kl}$ the resulting thermal strain components. p_{ijkl} are the elasto-optic coefficients. With the volume thermal expansion $\alpha = 1/V(\partial V/\partial T)_p = \kappa\gamma C_V/V$ within the anharmonic lattice theory one obtains

$$\delta\left(1/n^2\right)_{ij} = p_{ijkl}s_{ijkl}\gamma C_V\Delta T/V. \tag{2}$$

$\kappa = -V(\partial p/\partial V)_T = 1/\sum s_{ijkl}$ is the compression modulus with the compliances s_{ijkl}, γ the Grüneisen constant,

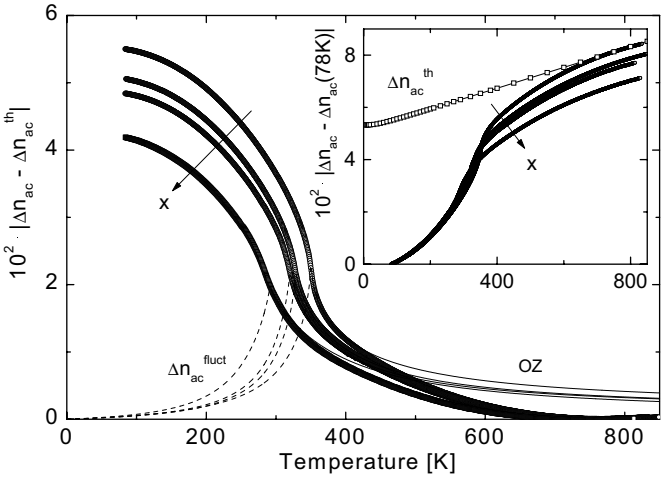

Fig. 1. Temperature dependencies of the principal linear birefringence Δn_{ac} of SBN61:Ce in the range $78 \leq T \leq 850$ K for Ce^{3+} concentrations $x = 0, 0.0066$, 0.0113 and 0.0207, respectively, as measured (inset) and after subtraction of the thermo-optic contribution Δn_{ac}^{th} (see text). The solid lines denoted as OZ refer to an Ornstein-Zernike analysis of the fluctuation induced LB tails at $T > T_c$ by fitting to equation (8) within the ranges $2\times10^{-3} < T/T_c - 1 < 5\times10^{-2}$. The dashed lines denote the Δn_{ac}^{fluc} data extrapolated to below T_c (see text).

C_V the specific heat capacity, V the volume and p the pressure. Within this simple approach one obtains

$$\Delta n_{ac}^{th} \propto U(T). \tag{3}$$

Here, $U(T) = \int C_V \mathrm{d}T$ is the internal lattice energy, which may be approximated by a 3D Debye-type function. Δn_{ac}^{th} as depicted in Figure 1 (inset) was approximated by equation (3) inserting a Debye temperature $\theta_D = 138$ K. This was calculated from the phononic contribution to the specific heat, $C_V^{phon}/T \propto T^2$, as measured on pure SBN at low temperatures [24]. Correct scaling to the LB data was obtained by fitting to the Debye curve between $T = 750$ and 800 K. After subtraction from the raw data one obtains the polarization-optic contribution, which is shown in Figure 1.

In the ferroelectric phase, the curves indicate saturation at low temperatures, $T < 100$ K. In the paraelectric regime one observes large tails extending over more than 300 K above T_c. These tails have their origin in the fluctuation behaviour of the order-parameter, which will be described below. The phase transitions are conspicuously smeared in SBN doped with Ce^{3+} in comparison with that of the pure SBN. This can clearly be seen in Figure 2, which shows the derivatives of the curves in Figure 1. The cusp-like minima denote the phase transition temperatures $T_c \approx 350$, 328, 320 and 291 K for the concentrations $x = 0$, 0.0066, 0.0113 and 0.0207, respectively. Interestingly, the cusp broaden and become rounded with increasing Ce^{3+} concentration. This might hint at the effect of random fields caused by local charge disorder, which increases with increasing Ce^{3+} dopants (see Sect. 4). Simultaneously the phase transitions are shifted towards lower temperatures.

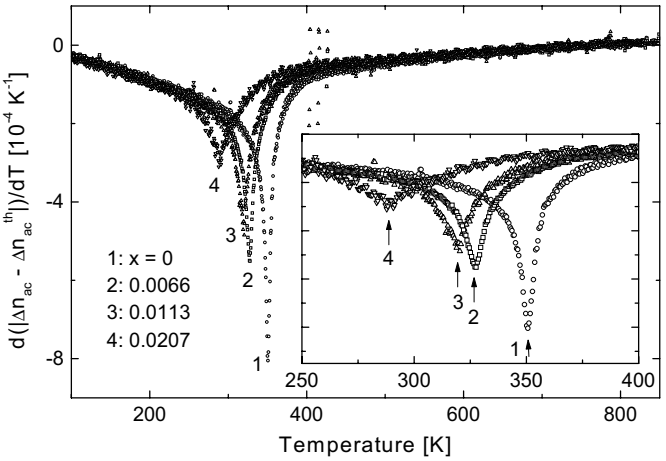

Fig. 2. Derivatives of the temperature dependent LB curves from Figure 1. The inset shows the details around the phase transition temperatures (arrows; see Tab. 1).

As mentioned above, the LB tails originate from the fluctuation behaviour of the order parameter **P** above T_c. Within the matrix notation of the indicatrix formalism [23] the variation of the dielectric impermeability can be expressed by

$$\delta\left(1/n^2\right)_i = \sum_{j=1}^{3} g_{ij}^{\mathrm{F}} P_j^2. \tag{4}$$

The g_{ij}^{F} are the free electro-optic coefficients including photoelastic contributions due to electrostriction. Within the tetragonal 4mm point symmetry the polarization-optic LB reads

$$\Delta n_{\mathrm{ac}} = -\left(n_0^3/2\right)\left(g_{11}^{\mathrm{F}} - g_{12}^{\mathrm{F}}\right)\langle P^2\rangle \tag{5}$$

with the time- and space-averaged autocorrelation function $\langle P^2\rangle = \langle P\rangle^2 + \langle \delta P^2\rangle$, where the squared order parameter is expected to vary as $\langle P\rangle^2 \propto (-t)^{2\beta}$ near to the phase transition at $T < T_c$ while $t = T/T_c - 1$ is the reduced temperature. Note that $\langle P\rangle = \langle P_z\rangle$ with $\hat{\mathbf{z}} \parallel \mathbf{c}$. n_0 denotes the average high-temperature refractive index. In the paraelectric regime, at $T > T_c$, the autocorrelation function $\langle P^2\rangle \equiv \langle \delta P^2\rangle$ is connected with the **q**-dependent susceptibility $\chi(\mathbf{q})$ *via* the fluctuation-dissipation theorem [25]

$$\langle \delta P^2\rangle = \left(k_{\mathrm{B}} T/8\pi^3\right) \int_0^{q_{\mathrm{m}}} \chi(\mathbf{q}) \mathrm{d}^3\mathbf{q}. \tag{6}$$

Within the Ornstein-Zernike approximation the susceptibility may be expanded for $q \to 0$ by

$$\chi(\mathbf{q}) = \chi(0)\left(1 + \xi^2 q^2\right)^{-1}, \tag{7}$$

where $\chi(0) = \varepsilon_0(\varepsilon - 1) \propto t^{-\gamma}$ is the static susceptibility and $\xi(t) = \xi_0^{\pm} t^{-\nu}$ the correlation length in the critical range. ν and γ represent the static critical exponents of the correlation length and the dielectric susceptibility, respectively. Replacing the cubic Brillouin zone by a sphere with $0 \le q \le q_{\mathrm{m}} = \pi/a$ (a = lattice constant) one obtains from equations (5–7) the fluctuation induced contribution to the LB,

$$\Delta n_{\mathrm{ac}}^{\mathrm{fluct}} = -\left(n_0^3 k_{\mathrm{B}} \varepsilon_0 q_{\mathrm{m}} T/4\pi^2 \xi_0^2\right)\left(g_{11}^{\mathrm{F}} - g_{12}^{\mathrm{F}}\right)|t|^{2\nu-\gamma} \times \left[1 - \tan^{-1}\left(q_{\mathrm{m}}\xi_0^{\pm}|t|^{-\nu}\right) / \left(q_{\mathrm{m}}\xi_0^{\pm}|t|^{-\nu}\right)\right]. \tag{8}$$

Equation (8) can directly be fitted to the high temperature tails of the LB. The solid lines in Figure 1 denoted as OZ are best fits using fitting ranges $2 \times 10^{-3} < T/T_c - 1 < 5 \times 10^{-2}$. The values for γ, ν and T_c thus obtained are shown in Table 1 and will be discussed below. By use of these values the dashed curves in Figure 1 are determined for the range $T < T_c$. Here the well-known ratio of the correlation lengths $\xi_0^+/\xi_0^- = \sqrt{1/2}$ (within Landau theory) has been introduced. After subtracting this contribution from the LB data one obtains their ferroelectric contributions, $\Delta n_{\mathrm{ac}}^{\mathrm{fe}}$, which are shown in Figure 3. In the vicinity of T_c their critical behaviour can be described by the well-known power law (solid lines in Fig. 3)

$$\Delta n_{\mathrm{ac}}^{\mathrm{fe}} \propto (-t)^{2\beta}. \tag{9}$$

As shown by the double-logarithmic plots in the inset of Figure 3 the chosen fitting ranges, $2 \times 10^{-3} < |T/T_c - 1| < 3 \times 10^{-2}$ (arrows), warrant clear power law behaviour by

Table 1. Best-fit parameters of the LB data shown in Figures 1 and 3 to equations (8) and (9), respectively.

x	ν	γ	β	T_c [K]
0.0	0.64 ± 0.13	1.30 ± 0.27	0.31 ± 0.01	350.2 ± 0.2
0.0066	0.69 ± 0.01	1.36 ± 0.02	0.35 ± 0.01	328.0 ± 0.1
0.0113	0.68 ± 0.86	1.34 ± 1.71	0.40 ± 0.01	320.0 ± 0.6
0.0207	0.79 ± 0.27	1.58 ± 0.51	0.46 ± 0.01	290.9 ± 1.3

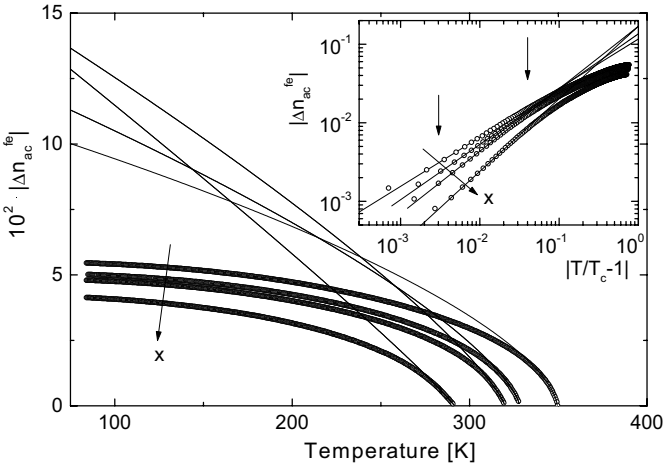

Fig. 3. Ferroelectric contribution of the LB, $\Delta n_{\mathrm{ac}}^{\mathrm{fe}}$, as obtained from the LB data in Figure 1 (see text) for the concentrations $x = 0, 0.0066,\ 0.0113$ and 0.0207, respectively. The data are fitted to equation (9) within the ranges $2 \times 10^{-3} < |T/T_c - 1| < 3 \times 10^{-2}$ (solid lines). Double-logarithmic plots and the fitting range (vertical arrows) are shown in the inset.

avoiding the curvature in the saturation range at $|t| > 0.05$. The best fitted values for β are included in Table 1.

4 Discussion

All critical exponents obtained for pure SBN61, $\gamma = 1.30 \pm 0.27$, $\nu = 0.64 \pm 0.13$ and $\beta = 0.31 \pm 0.01$, comply with those of the three-dimensional (3D) Ising model, where $\gamma = 1.24$, $\nu = 0.63$ and $\beta = 0.325$ are expected. This result agrees with the assumption of a one-dimensional order parameter in this uniaxial system. Owing to the inherent disorder of SBN61 one might argue that it should rather comply with the 3D random bond Ising model (RBIM). However, the RBIM exponent $\beta = 0.349$ [26] is not significantly different from the value observed on SBN61. Hence, both models seem to describe the observed critical behaviour equally well. Similarly, the 3D RBIM exponents $\nu = 0.68$ and $\gamma = 1.39$ [26] do not contradict within errors those observed on SBN61.

Upon doping with Ce^{3+} charge disorder is encountered, giving rise to random dipolar fields. They are probably due to Ce^{3+}-V_0 centers, since Ce^{3+} generally occupies Sr^{2+} lattice sites [11] and thus will create nearby oxygen vacancies. As a consequence, we believe, the values for γ and ν are shifted to higher values against those of the 3D random-field Ising model (RFIM), where $\gamma = 1.75$ and $\nu = 1$ are expected [21]. In this limit, however, rounding effects due to the well-known [27] extreme critical slowing-down will prevent reliable measurements of criticality in the paraelectric regime, $T > T_c$. In the present study such rounding has been observed very close to T_c (see Fig. 2, inset), but could be excluded from the analysis by the above choice of the fitting interval. Its lower bound will drastically increase when increasing x to above 0.2, and thus finally rule out critical point analysis in the true RFIM limit.

Surprisingly, the critical exponent β tends to achieve rather high values, $\beta \to 0.5$ (Tab. 1), in disagreement with the expected RFIM value $\beta \cong 0$ [21]. We believe this behaviour to be due to domain disorder as a consequence of the quenched RFs. Basically, the ferroelectric domain structure occurring below T_c is expected to become increasingly fine-grained when increasing the concentration, x [28]. However, since the 3D RFIM exhibits long-range ordering in thermodynamic equilibrium [19], domain growth takes place just below T_c on a logarithmic time scale [28]. Hence, upon slowly cooling to below T_c finally a coarsened domain structure will appear, with domain sizes, R, coming close to those in pure SBN61. This will change, however, upon heating towards T_c again. In the fluctuation range very probably roughening of previously flat domain walls and, finally, a decay into nanodomains will take place. As a result, this inherent disorder gives rise to a decrease of the average order parameter, $\langle P \rangle$. A global measurement of $\langle P \rangle^2$ as effectuated by the LB method will then feel a stronger decrease than that of the local order parameter existing in the bulk of the domains. As a consequence one observes enhanced values of the effective "critical" exponent, β. A similar explanation may hold in the case of the structural RFIM $DyAs_xV_{1-x}O_4$, where domain wall roughening has been observed in the ordered phase [29] and $\beta \approx 0.31$ [30] disagrees with RFIM expectations.

5 Conclusion

The LB measurements made on SBN61:Ce have shown that relaxor behaviour prevails in the precursor regime at $T > T_c$. These relaxor properties can be explained by spatial fluctuations of local RFs. They may cause some smearing of the ferroelectric phase transition even though a sharp phase transition is expected in an Ising system with weak RFs in thermodynamic equilibrium. A critical point analysis of the LB data yields that the pure SBN61 seems to belong to the 3D Ising universality class. Doping with Ce^{3+} enhances the relaxor properties and drives the system towards the RFIM.

At $T < T_c$ a ferroelectric domain state is encountered. Domain wall roughening due to interactions with RFs seems to prohibit the determination of the critical behaviour of the order parameter below T_c. In order to check this conjecture it will be interesting to study the relaxation kinetics of domains in SBN61 in the vicinity of T_c in future investigations.

Work supported by Deutsche Forschungsgemeinschaft within the framework of the Schwerpunktprogramm "Strukturgradienten in Kristallen" and Sonderforschungsbereich 225.

References

1. A.M. Glass, J. Appl. Phys. **40**, 4699 (1969).
2. R.R. Neurgoankar, M.H. Kalisher, T.C. Lim, E.J. Staples, K.L. Keester, Mater. Res. Bull. **15**, 1235 (1980).
3. K. Tada, T. Murai, M. Aoki, K. Muto, K. Awazu, Jpn J. Appl. Phys. **11**, 1622 (1972).
4. R.R. Neurgoankar, W.K. Cory, J.R. Oliver, Ferroelectrics **51**, 3 (1983).
5. B. Fisher, M. Cronin-Golomb, J.O. White, A. Yariv, R.R. Neurgoankar, Appl. Phys. Lett. **40**, 863 (1982).
6. G. Salamon, M.J. Miller, W.W. Clark III, G.L. Wood, E.J. Sharp, Opt. Commun. **59**, 417 (1986).
7. R.R. Neurgoankar, W.K. Cory, J. Opt. Soc. Am. B **3**, 274 (1986).
8. R.R. Neurgoankar, W.K. Cory, J.R. Oliver, M.D. Ewbank, W.F. Hall, Opt. Eng. **26**, (1987).
9. S.C. Abrahams, P.B. Jamieson, J.L. Bernstein, J. Chem. Phys. **54**, 2355 (1971).
10. K. Megumi, N. Nagatsuma, K. Kashiwada, Y. Furuhata, Mater. Sci. **11**, 1583 (1976).
11. Th. Woike, G. Weckwerth, H. Palme, R. Pankrath, Solid State Commun. **102**, 743 (1997).
12. Th. Woike, T. Volk, U. Dörfler, R. Pankrath, L. Ivleva, M. Wöhlecke, Ferroelectrics Lett. **23**, 127 (1998).
13. G. Burns, F.H. Dacol, Solid State Commun. **58**, 567 (1986).

14. T. Heinz, G. Burns, N. Halas, Bull. Am. Phys. Soc. **31**, 603 (1986).
15. P. Lehnen, J. Dec, W. Kleemann, Th. Woike, R. Pankrath, Ferroelectrics (in press).
16. J. Dec, W. Kleemann, Th. Woike, R. Pankrath, Eur. Phys. J. B **14**, 627 (2000).
17. Y.G. Wang, W. Kleemann, Th. Woike, R. Pankrath, Phys. Rev. B **61**, 3333 (2000).
18. V. Westphal, W. Kleemann, M.D. Glinchuk, Phys. Rev. Lett. **68**, 847 (1992); W. Kleemann, Int. J. Mod. Phys. B **7**, 2469 (1993).
19. Y. Imry, S.K. Ma, Phys. Rev. Lett. **35**, 1399 (1975).
20. R. Blinc, J. Dolinsek, A. Gregorovic, B. Zalar, C. Filipic, Z. Kutnjak, A. Levstik, R. Pirc, Phys. Rev. Lett. **83**, 424 (1999); R. Pirc, R. Blinc, Phys. Rev. B **60**, 13470 (1999).
21. D. Belanger, A. Young, J. Magn. Magn. Mater. **100**, 272 (1991).
22. W. Kleemann, F.J. Schäfer, J. Nouet, Physica **97B**, 145 (1979).
23. J.F. Nye, *Physical Properties of Crystals* (Oxford University Press, Oxford, 1960).
24. J.J. de Yoreo, R.O. Pohl, G. Burns, Phys. Rev. B **32**, 5780 (1985).
25. W. Kleemann, F.J. Schäfer, M.D. Fontana, Phys. Rev. B **30**, 1148 (1984).
26. G. Jug, Phys. Rev. B **27**, 609 (1983).
27. J. Villain, J. Phys. France **46**, 1843 (1985); D.S. Fisher, Phys. Rev. Lett. **56**, 416 (1986).
28. J. Villain, Phys. Rev. Lett. **52**, 1543 (1984); G. Grinstein, J.F. Fernandez, Phys. Rev. B **29**, 6389 (1984).
29. J.T. Graham, D.R. Taylor, D.R. Noakes, W.J.L. Buyers, Phys. Rev. B **43**, 3778 (1991).
30. D.R. Taylor, K.A. Reza, J. Magn. Magn. Mater. **104–107** (1992).